Strong Coupling of Two Individually Controlled Atoms via a Nanophotonic Cavity

Polnop Samutpraphoot,[1,*] Tamara Đorđević,[1,*] Paloma L. Ocola,[1,*] Hannes Bernien,[2] Crystal Senko,[3,4] Vladan Vuletić,[5] and Mikhail D. Lukin[1,†]

[1]*Department of Physics, Harvard University, Cambridge, Massachusetts 02138, USA*
[2]*Pritzker School of Molecular Engineering, University of Chicago, Chicago, Illinois 60637, USA*
[3]*Department of Physics and Astronomy, University of Waterloo, Waterloo, Ontario N2L 3R1, Canada*
[4]*Institute for Quantum Computing, University of Waterloo, Waterloo, Ontario N2L 3R1, Canada*
[5]*Department of Physics and Research Laboratory of Electronics, Massachusetts Institute of Technology, Cambridge, Massachusetts 02139, USA*

(Received 19 September 2019; accepted 5 December 2019; published 11 February 2020)

We demonstrate photon-mediated interactions between two individually trapped atoms coupled to a nanophotonic cavity. Specifically, we observe collective enhancement when the atoms are resonant with the cavity and level repulsion when the cavity is coupled to the atoms in the dispersive regime. Our approach makes use of individual control over the internal states of the atoms and their position with respect to the cavity mode, as well as the light shifts to tune atomic transitions individually, allowing us to directly observe the anticrossing of the bright and dark two-atom states. These observations open the door for realizing quantum networks and studying quantum many-body physics based on atom arrays coupled to nanophotonic devices.

DOI: 10.1103/PhysRevLett.124.063602

Controlled interactions between individual photons and quantum emitters are an important ingredient for the realization of scalable quantum information systems [1,2]. Nanophotonic devices in which the light is confined to subwavelength dimensions constitute a promising approach for engineering strong light-matter coupling [3,4]. The appeal of a nanophotonic platform is due to two key features. On one hand, nanophotonic devices allow the photonic dispersion to be tailored to achieve tunable-range interactions between coupled emitters [5–10] and engineer a range of interaction Hamiltonians [11,12]. On the other hand, the nanoscale mode volume enables an efficient high-cooperativity emitter-photon interface suitable for realizing potentially scalable systems [13–17]. In particular, cold neutral atoms have recently emerged as a promising approach for realizing large-scale quantum systems due to the ability to generate large numbers of identical individually trapped atoms [18–23]. While significant effort is currently being directed toward coupling multiple isolated atoms to nanophotonic systems [7,24–26], achieving a strong coupling of a deterministic number of atoms remains a challenge. The atoms must be trapped closely enough to the device to maximize the coupling within the evanescent field, while overcoming attractive surface forces [27,28] and preserving the excellent atomic coherence properties.

In this Letter, we report on the observation of strong coupling of two individually controlled atoms via a nanophotonic cavity. In particular, we spectroscopically demonstrate collective enhancement in the resonant regime and level repulsion in the dispersive regime. These experiments utilize individual control of the positions of the atoms with respect to the cavity mode, their internal states, and the frequencies of their transitions. This allows us to observe the anticrossing of the bright and dark two-atom states, in analogy to prior observations involving superconducting qubits and color centers in diamond [29,30].

Our experiments utilize a cavity QED system consisting of ^{87}Rb atoms coupled to the evanescent field of a photonic crystal (PC) cavity [Figs. 1(a) and 1(b)] [7]. The SiN nanophotonic device is suspended in a vacuum chamber on a tapered optical fiber, which is also used for efficient interrogation of the cavity by exciting and collecting photons through its fiber-optic interface [31]. This approach minimizes the physical footprint of the system, thus allowing for good optical access and unobstructed trapping and cooling, while retaining the flexibility to control the atomic position and confinement. The atoms are trapped using tightly focused optical tweezers that localize them to within tens of nanometers and can be steered to desired locations. The internal states of the atoms are individually manipulated with light fields copropagating with the optical tweezers. We interrogate the response of the atom-cavity system by scanning the frequency of the probe field to measure the reflection spectrum. The frequency of the cavity is tuned thermally with a laser beam pointed at the heater pad [Fig. 1(c)].

We probe the atom-cavity spectrum by tuning the cavity to the $5S_{1/2} \rightarrow 5P_{3/2}$ transition at 780 nm. The spectrum is acquired by scanning the probe field from the ground state manifold $5S_{1/2}, F = 2$ across the excited state manifolds

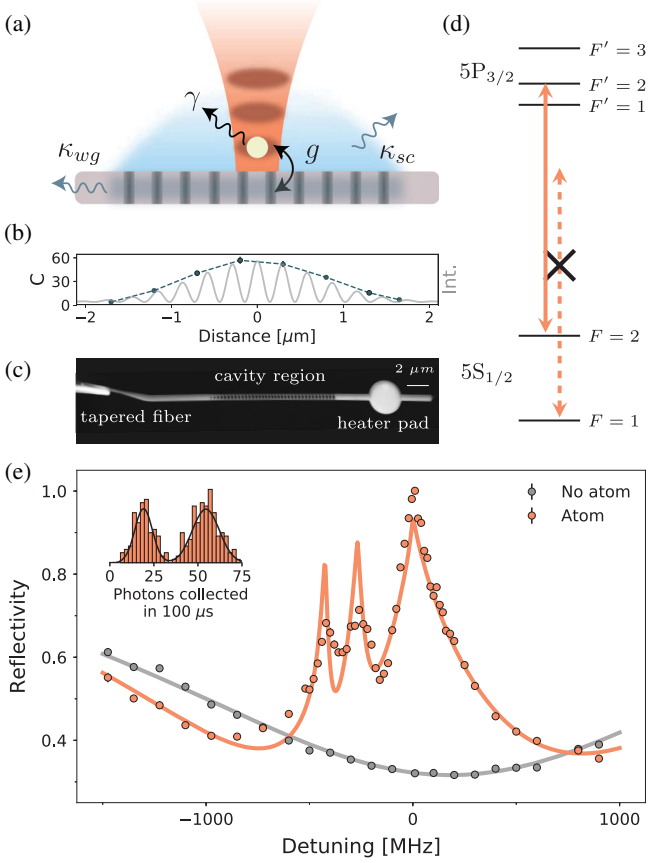

FIG. 1. High-cooperativity atom-photon coupling to a nanophotonic cavity. (a) Schematic of the experimental setup, showing an atom trapped in the lattice of an optical tweezer coupled to a nanophotonic cavity. The parameters are defined in the main text. (b) Moving the tweezer along the cavity to map out the mode in terms of cooperativity (blue) and simulated intensity profile of the cavity mode (gray). (c) SEM image of the nanophotonic cavity suspended on a tapered fiber. (d) Level diagram for the $5S_{1/2} \rightarrow 5P_{3/2}$ transition. The $F = \{2, 1\}$ manifold is {coupled, uncoupled} to the cavity. The probe detuning is defined relative to the bare $F = 2 \rightarrow F' = 3$ transition. (e) Measured cavity reflection spectrum with and without an atom coupled to the cavity. The solid lines are from theoretical models. (Inset) Histogram of counts collected at 0 MHz detuning, showing single-shot atomic detection.

$5P_{3/2}, F' = 1, 2, 3$ [Fig. 1(d)], while the atom is positioned at the center of the cavity mode. We note that, for all the spectra presented in this Letter, the probe detuning is relative to the bare $F = 2 \rightarrow F' = 3$ transition, and the error bars are obtained from statistical uncertainties acquired over multiple experimental runs.

Figure 1(e) shows the reflection spectrum of the cavity with and without an atom present. For the case without an atom, the reflection spectrum is a resonance dip of the empty cavity. The presence of an atom drastically changes the spectrum, and we observe three atomic lines that are significantly broadened due to resonant coupling between the atom and the cavity. This effect is described by the Purcell enhancement. In the resonant regime, the radiative decay rate into the cavity mode is enhanced by the single-atom cooperativity $C = 4g^2/\kappa\gamma$, where g is the single-photon Rabi frequency and γ is the atomic spontaneous decay rate. The cavity decays at the rate κ_{wg} into the waveguide and κ_{sc} elsewhere, yielding the total cavity decay rate $\kappa = \kappa_{\mathrm{wg}} + \kappa_{\mathrm{sc}}$ [Fig. 1(a)]. The observed line shape is accurately described using a model incorporating a distribution of cooperativities, rather than a single-valued one. Taking these considerations into account, we fit the spectrum in Fig. 1(e) and extract the average cooperativity $C = 71(4)$, corresponding to the cavity QED parameters $\{2g, \gamma, \kappa_{\mathrm{wg}}, \kappa_{\mathrm{sc}}\} = 2\pi \times \{1.24(4), 0.006, 0.86, 2.77\}$ GHz. We compare this to an independent theoretical estimate of g based on the geometry of the trapping potential of the tweezer and the evanescent field experienced by the atom. The closest lattice site is at a distance of 260 nm from the surface of the PC [7]. At this distance, an atom at rest experiences a single-photon Rabi frequency of $2g_0 = 2\pi \times 1.7$ GHz, which is somewhat larger than the observed values.

We attribute this discrepancy to the fluctuations in the atomic position across the spatially varying cavity field, which lead to cooperativity distributions. The distribution of cooperativities that produces the spectrum in Fig. 1(e) corresponds to the atomic spatial widths of 190 nm along the PC and 33 nm along the direction of propagation of the tweezer. An independent temperature measurement yields an upper bound estimate of 120 μK near the PC, accounting for 150 and 30 nm in the two directions, respectively (see Supplemental Material [32]). Other contributions include the pointing fluctuations of the tweezer. Both of these fluctuations affect the line shapes of the spectra shown in this Letter and make the cavity standing wave profile unresolvable [Fig. 1(b)]. With these position fluctuations, we estimate an average single-photon Rabi frequency of $2g = 2\pi \times 1.26$ GHz, which is consistent with the value extracted from our experimental data.

The efficient atom-photon interface allows us to determine the presence of an atom in a single shot. We tune the probe frequency to the $F = 2 \rightarrow F' = 3$ line and count reflected photons collected within 100 μs [Fig. 1(e), inset]. When repeated multiple times, the photon number follows a bimodal normal distribution with 0.7% overlap, which is adequately separable to determine if the atom is coupled to the cavity. The atom becomes uncoupled from the cavity if it falls into the $F = 1$ manifold via off-resonant scattering. We deplete the population in the $F = 1$ manifold by sending in an additional beam copropagating with the optical tweezer on the $5S_{1/2}$, $F = 1 \rightarrow 5P_{1/2}$, $F' = 2$ transition, at 795 nm, which is sufficiently detuned from the cavity and can be filtered out from the collected photons. In addition to the $F = 2 \rightarrow F' = 3$ line, the spectrum in Fig. 1(e) also shows the $F = 2 \rightarrow F' = 1, 2$

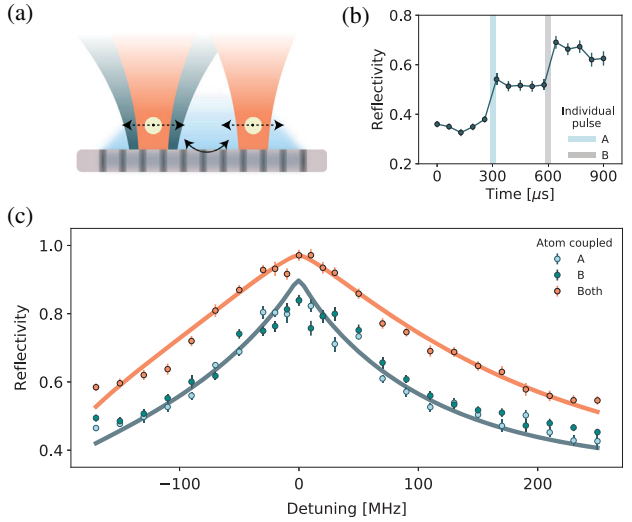

FIG. 2. Individual control and resonant coupling. (a) Illustration of the individual position and internal state control with a repumping (blue) beam copropagating with one of the optical tweezers (orange). (b) Average reflectivity jumps after pumping each atom to the $F = 2$ manifold, taken at the probe detuning of 100 MHz. (c) Broadening of the $F = 2 \rightarrow F' = 3$ line. The labels A and B denote the atoms in the two tweezers. The spectrum is taken when the tweezers are positioned 1 μm away from the mode center to retain addressability. The solid lines are from theoretical models.

transitions, which are not cycling and would not be visible without applying the repumping beam.

The reflection spectrum is used to study the cooperativity dependence on experimental parameters, such as the position of the atom. Taking advantage of the individual position control, we scan the tweezer position along the axis of the PC by steering the galvanometer mirrors and acquire a spectrum associated with each position (see Supplemental Material [32]). We then determine the cooperativity at each location from the Purcell-enhanced linewidth and find that the resulting cooperativity dependence [Fig. 1(b), blue] traces out the envelope of the numerically simulated field profile intensity (gray).

Having characterized the single-atom coupling, we now turn to the case of two atoms to study their resonant coupling via the cavity [Fig. 2(a)]. The two tweezers must be placed away from each other to avoid overlap and cross talk, hence inevitably lowering their individual cooperativities. The experiments involving two atoms are operated with the tweezers placed 1 μm away from the mode center, corresponding to the average single-atom cooperativity $C = 31(2)$ [Fig. 1(b), blue], well within the strong coupling regime.

In addition to the position control, the two-atom experiments also make use of internal state manipulation of individual atoms. This is achieved by having repumping beams copropagating with the tweezers, selectively bringing the desired atom into the $F = 2$ manifold. We demonstrate this by applying 3 μs long repumping pulses at 300 μs on one tweezer and 600 μs on the other, while constantly probing the spectrum with the probe blue detuned to 100 MHz and monitoring the collected photon counts in time [Fig. 2(b)]. The average collected counts step up following each pulse, indicating the influence of repumping the atoms one at a time. The capability of individual repumping is utilized for detection and post-selection on having two atoms coupled to the cavity in each trial of the experiment (see Supplemental Material [32]).

With these capabilities, we explore the collective behavior of two atoms simultaneously coupled to the cavity by acquiring a reflection spectrum centered on the $F = 2 \rightarrow F' = 3$ line [Fig. 2(c), orange]. We observe broadening of the spectrum in the two-atom case. The spectrum is well described by our theoretical model, generated using the sum of individual cooperativities extracted from the single-atom spectra with no additional parameters (see Supplemental Material [32]). We extract the full width at half maximum of $2\pi \times \{170, 300\}$ MHz for the case of {one, two} atom(s) coupled to the cavity. The effect of line

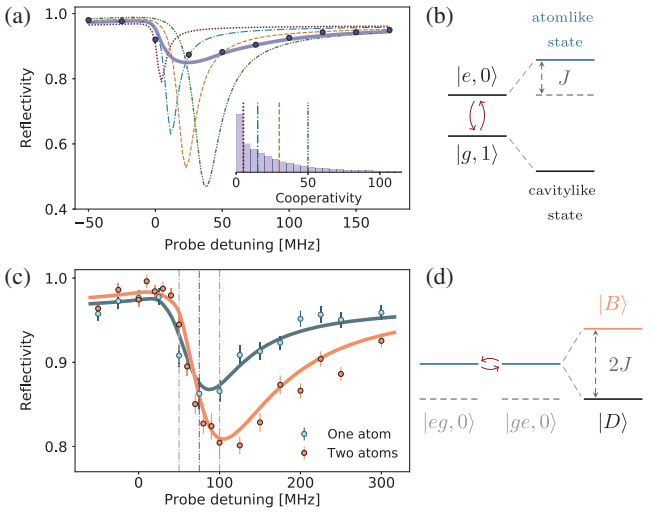

FIG. 3. Atom-photon interaction in the dispersive regime. (a) Atomlike spectrum of the $F = 2 \rightarrow F' = 3$ line at cavity detuning $\Delta = 2\kappa$. Theoretical curves (dashed-dotted) generated with single-valued cooperativities (vertical lines, inset). Theoretical curve (solid) constructed using cooperativity distribution (inset). This spectrum is acquired without a light shift from the tweezer. (b) Level diagram of one atom in the singly excited manifold. Bare states with {atomic, photonic} excitation $\{|e,0\rangle, |g,1\rangle\}$ are dressed by the atom-photon coupling $J = g^2/\Delta$ into the {atom, cavity}-like components. (c) Single- and two-atom spectra when the two atoms are resonant with each other. The vertical lines delineate the frequency of an atom in a 50 MHz deep tweezer not coupled to the cavity (gray) and the expected cavity-induced shifts of the {one, two} atom(s) coupled to the cavity {blue, orange}. (d) Level diagram of two atoms. The two atomlike components hybridize into the {dark, bright} states $\{|D\rangle, |B\rangle\}$, which experience frequency shifts of $\{0, 2J\}$. The solid lines are theoretical models.

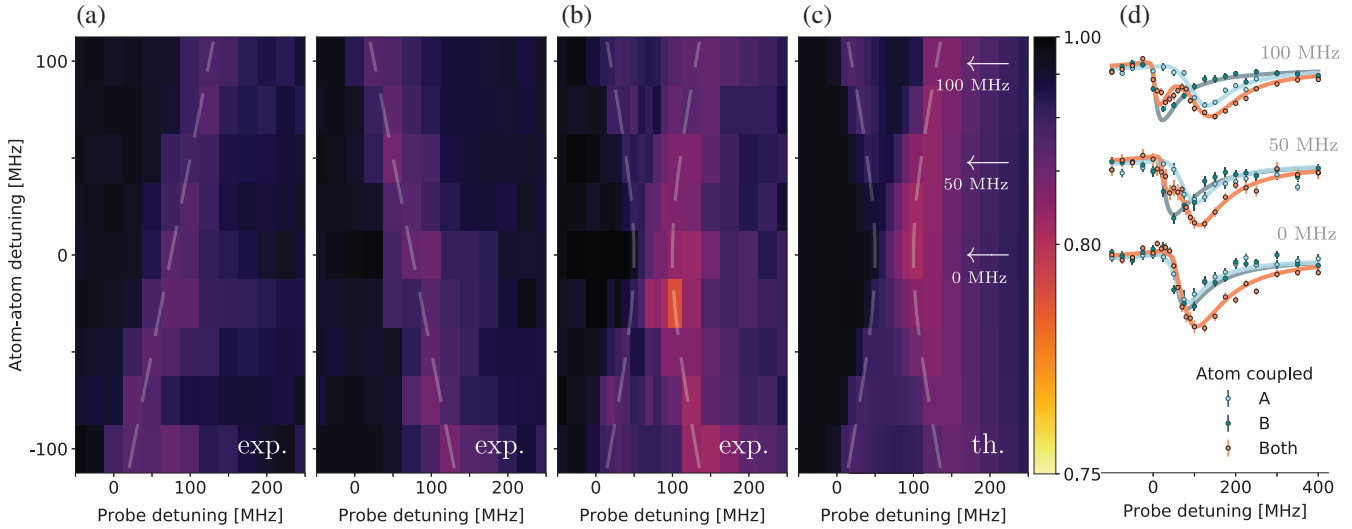

FIG. 4. Level repulsion of the atomic lines induced by the cavity-mediated interaction. Experimental data of reflectivity map over probe detuning and relative atom detuning δ_{AB} for (a) individual atoms coupled to the cavity, plotted with their expected light shifted frequencies (dashed lines) and (b) two atoms simultaneously coupled to the cavity, plotted with frequencies of the bright and dark states (dashed lines), showing level repulsion. (c) Theoretical calculation for two atoms simultaneously coupled to the cavity. (d) Cross sections of the reflectivity map showing single- and two-atom spectra at $\delta_{AB} = 2\pi \times \{0, 50, 100\}$ MHz indicated by the white arrows in (c), plotted with theoretical models (solid lines).

broadening can be interpreted as a result of collective enhancement [24,41].

The phenomena described above, such as the Purcell effect and collective enhancement, can also be demonstrated spectroscopically in the dispersive regime. We red detune the cavity relative to the $F = 2 \rightarrow F' = 3$ line by $\Delta = 2\kappa$ and acquire a single-atom spectrum [Fig. 3(a)]. We observe that the atomic line becomes narrower than the resonant case and experiences a frequency shift [42]. The shift is a result of the atom-cavity interaction in the dispersive regime [Fig. 3(b)]. In this regime, the atom is dressed by the cavity coupling and experiences a frequency shift of $g^2/\Delta = C\kappa\gamma/4\Delta$, while its Purcell-enhanced linewidth is suppressed by a factor of $1 + 4\Delta^2/\kappa^2$.

In the same manner as the resonant case, the experimental data cannot be adequately captured by theoretical curves [Fig. 3(a), dashed-dotted lines] generated with single-valued cooperativities [Fig. 3(a), inset, vertical lines], but is rather well described using a model involving the cooperativity distribution shown in the inset of Fig. 3(a). This distribution leads to varying frequency shifts, which result in additional broadening and modified line shape.

The collective coupling in the dispersive regime can be characterized by probing spectra at a cavity detuning with one and two atom(s) at the same resonance frequency [Fig. 3(c)]. The single-atom shift is consistent with the expected value of $J = 2\pi \times 25(4)$ MHz based on our average cooperativity estimate from the theoretical model describing the spectrum in Fig. 2(c). The two-atom spectrum appears as a single line that experiences a shift twice as large as the single-atom line [43].

The twofold enhancement of the frequency shift can be understood as level repulsion between the two collective atomic states [Fig. 3(d)]. These states are the symmetric and antisymmetric superpositions of the two-atom states. The symmetric superposition interacts more strongly with the cavity due to constructive interference of coherent scattering into the cavity mode, thereby experiencing the frequency shift of $2g^2/\Delta$ and forming the bright state $|B\rangle = (|eg, 0\rangle + |ge, 0\rangle)/\sqrt{2}$. The antisymmetric superposition does not interact with the cavity due to the destructive interference, acquires zero shift, and forms the dark state $|D\rangle = (|eg, 0\rangle - |ge, 0\rangle)/\sqrt{2}$. The difference in their frequency shifts results in line splitting, which can be equivalently viewed as an interaction between two atoms with coupling rate $2J = 2g^2/\Delta$ due to an off-resonant exchange of virtual cavity photons [24].

We further illustrate the dynamics of level repulsion by tuning the atoms in and out of resonance with each other. The relative atom detuning $\delta_{AB} = \delta_A - \delta_B$ is tuned with the light shifts induced by the individual tweezers, in our case, within $2\pi \times (\pm 100$ MHz) [Fig. 4(a)] (see Supplemental Material [32]). As we tune from large δ_{AB} toward zero with both atoms coupled to the cavity [Figs. 4(b) and 4(d)], we observe avoided crossing in the two-atom spectrum. The relative intensities of the lines are modified as the dark and bright components are mixed. At $\delta_{AB} = 0$, the dark component disappears, and the bright component experiences a twofold shift. The frequencies of the lines follow $\sqrt{(2J)^2 + \delta_{AB}^2}$ with the gap that signifies the coupling strength of $2J = 2\pi \times 50(8)$ MHz, in agreement with the theoretical analysis shown in Fig. 4(c).

The observations demonstrate a controllable high-cooperativity interface between atoms and photons, as well as between two atoms mediated by virtual cavity photons, namely, collective enhancement and anticrossing. These results can be extended along several directions.

First, the photon-mediated interactions can be combined with coherent quantum control of the internal states of the atoms to implement quantum gates for state transfer and entanglement generation [44–47]. As the errors of many of the protocols for these applications decrease with larger cooperativity, further improvement in cooperativity is an essential prerequisite for scalability. This may be achieved by positioning the atoms closer to the surface to access a larger field strength [48], improving the design and fabrication of the nanophotonic devices [49], or cooling the atoms for tighter localization with respect to the mode maxima [50–52]. Second, this approach offers a complete toolbox for controlling quantum many-body systems. The number of atoms can be scaled up by generating tweezer arrays [18–23]. The established techniques for assembling atom arrays can be combined with our approach for the individual addressing and light shift control and recently developed techniques for imaging an array on a nanophotonic structure [25]. Combining these capabilities with the ability to engineer band dispersion may allow for the exploration of novel many-body systems with extensive tunability. Finally, the efficient high-bandwidth atom-photon interface with individual atomic control is naturally suitable for realizing quantum networks with multiqubit nodes [53–55]. The nanoscale interface also holds prospects of integration with modular architecture such as on-chip photonic circuits and fiber-optic networks for various applications ranging from quantum repeaters to distributed quantum computing [56,57].

We thank Rivka Bekenstein, Robert Bettles, Johannes Borregaard, Manuel Endres, Hannes Pichler, Florentin Reiter, Sylvain Schwartz, François Swiadek, Jeff Thompson, Susanne Yelin, and Alexander Zibrov for useful discussions and experimental contributions. This work was supported by the Center for Ultracold Atoms (Grant No. PHY-1125846), the National Science Foundation (Grant No. PHY-1506284), AFOSR (Grant No. FA9550-16-1-0323), Vannevar Bush Faculty Fellowship (Grant No. N00014-15-1-2846), and ARL CDQI (Grant No. W911NF1520067).

*These authors contributed equally to this work.
†lukin@physics.harvard.edu

[1] D. P. DiVincenzo, Fortschr. Phys. **48**, 771 (2000).
[2] A. Reiserer and G. Rempe, Rev. Mod. Phys. **87**, 1379 (2015).
[3] P. Lodahl, S. Mahmoodian, and S. Stobbe, Rev. Mod. Phys. **87**, 347 (2015).
[4] D. E. Chang, J. S. Douglas, A. González-Tudela, C.-L. Hung, and H. J. Kimble, Rev. Mod. Phys. **90**, 031002 (2018).
[5] P. Lodahl, A. Floris van Driel, I. S. Nikolaev, A. Irman, K. Overgaag, D. Vanmaekelbergh, and W. L. Vos, Nature (London) **430**, 654 (2004).
[6] D. Englund, A. Majumdar, A. Faraon, M. Toishi, N. Stoltz, P. Petroff, and J. Vučkovič, Phys. Rev. Lett. **104**, 073904 (2010).
[7] J. D. Thompson, T. G. Tiecke, N. P. de Leon, J. Feist, A. V. Akimov, M. Gullans, A. S. Zibrov, V. Vuletić, and M. D. Lukin, Science **340**, 1202 (2013).
[8] A. Sipahigil, R. E. Evans, D. D. Sukachev, M. J. Burek, J. Borregaard, M. K. Bhaskar, C. T. Nguyen, J. L. Pacheco, H. A. Atikian, C. Meuwly, R. M. Camacho, F. Jelezko, E. Bielejec, H. Park, M. Lončar, and M. D. Lukin, Science **354**, 847 (2016).
[9] E. Miyazono, T. Zhong, I. Craiciu, J. M. Kindem, and A. Faraon, Appl. Phys. Lett. **108**, 011111 (2016).
[10] A. M. Dibos, M. Raha, C. M. Phenicie, and J. D. Thompson, Phys. Rev. Lett. **120**, 243601 (2018).
[11] J. S. Douglas, H. Habibian, C. L. Hung, A. V. Gorshkov, H. J. Kimble, and D. E. Chang, Nat. Photonics **9**, 326 (2015).
[12] A. González-Tudela, C. L. Hung, D. E. Chang, J. I. Cirac, and H. J. Kimble, Nat. Photonics **9**, 320 (2015).
[13] L.-M. Duan and H. J. Kimble, Phys. Rev. Lett. **92**, 127902 (2004).
[14] T. G. Tiecke, J. D. Thompson, N. P. de Leon, L. R. Liu, V. Vuletić, and M. D. Lukin, Nature (London) **508**, 241 (2014).
[15] L.-M. Duan and H. J. Kimble, Phys. Rev. Lett. **90**, 253601 (2003).
[16] H.-J. Briegel, W. Dür, J. I. Cirac, and P. Zoller, Phys. Rev. Lett. **81**, 5932 (1998).
[17] L. M. Duan, M. D. Lukin, J. I. Cirac, and P. Zoller, Nature (London) **414**, 413 (2001).
[18] H. Kim, W. Lee, H.-g. Lee, H. Jo, Y. Song, and J. Ahn, Nat. Commun. **7**, 13317 (2016).
[19] M. Endres, H. Bernien, A. Keesling, H. Levine, E. R. Anschuetz, A. Krajenbrink, C. Senko, V. Vuletic, M. Greiner, and M. D. Lukin, Science **354**, 1024 (2016).
[20] D. Barredo, S. de Léséleuc, V. Lienhard, T. Lahaye, and A. Browaeys, Science **354**, 1021 (2016).
[21] D. Barredo, V. Lienhard, S. de Léséleuc, T. Lahaye, and A. Browaeys, Nature (London) **561**, 79 (2018).
[22] A. Kumar, T.-Y. Wu, F. Giraldo, and D. S. Weiss, Nature (London) **561**, 83 (2018).
[23] D. Ohl de Mello, D. Schäffner, J. Werkmann, T. Preuschoff, L. Kohfahl, M. Schlosser, and G. Birkl, Phys. Rev. Lett. **122**, 203601 (2019).
[24] A. Goban, C.-L. Hung, J. D. Hood, S.-P. Yu, J. A. Muniz, O. Painter, and H. J. Kimble, Phys. Rev. Lett. **115**, 063601 (2015).
[25] M. E. Kim, T.-H. Chang, B. M. Fields, C.-A. Chen, and C.-L. Hung, Nat. Commun. **10**, 1647 (2019).
[26] E. Vetsch, D. Reitz, G. Sagué, R. Schmidt, S. T. Dawkins, and A. Rauschenbeutel, Phys. Rev. Lett. **104**, 203603 (2010).
[27] M. Antezza, L. P. Pitaevskii, and S. Stringari, Phys. Rev. A **70**, 053619 (2004).
[28] J. M. Obrecht, R. J. Wild, and E. A. Cornell, Phys. Rev. A **75**, 062903 (2007).
[29] J. Majer, J. M. Chow, J. M. Gambetta, J. Koch, B. R. Johnson, J. A. Schreier, L. Frunzio, D. I. Schuster, A. A. Houck, A. Wallraff, A. Blais, M. H. Devoret, S. M. Girvin, and R. J. Schoelkopf, Nature (London) **449**, 443 (2007).

[30] R. E. Evans, M. K. Bhaskar, D. D. Sukachev, C. T. Nguyen, A. Sipahigil, M. J. Burek, B. Machielse, G. H. Zhang, A. S. Zibrov, E. Bielejec, H. Park, M. Lončar, and M. D. Lukin, Science **362**, 662 (2018).
[31] T. G. Tiecke, K. P. Nayak, J. D. Thompson, T. Peyronel, N. P. de Leon, V. Vuletić, and M. D. Lukin, Optica **2**, 70 (2015).
[32] See Supplemental Material at http://link.aps.org/supplemental/10.1103/PhysRevLett.124.063602, which includes Refs. [33–40], for experimental methods and theoretical model.
[33] E. R. Abraham and E. A. Cornell, Appl. Opt. **37**, 1762 (1998).
[34] S. Gröblacher, J. T. Hill, A. H. Safavi-Naeini, J. Chan, and O. Painter, Appl. Phys. Lett. **103**, 181104 (2013).
[35] J. Chan, M. Eichenfield, R. Camacho, and O. Painter, Opt. Express **17**, 3802 (2009).
[36] E. D. Black, Am. J. Phys. **69**, 79 (2001).
[37] N. Schlosser, G. Reymond, and P. Grangier, Phys. Rev. Lett. **89**, 023005 (2002).
[38] D. Hümmer, P. Schneeweiss, A. Rauschenbeutel, and O. Romero-Isart, Phys. Rev. X **9**, 041034 (2019).
[39] K. M. Birnbaum, A. S. Parkins, and H. J. Kimble, Phys. Rev. A **74**, 063802 (2006).
[40] S. Kuhr, W. Alt, D. Schrader, I. Dotsenko, Y. Miroshnychenko, A. Rauschenbeutel, and D. Meschede, Phys. Rev. A **72**, 023406 (2005).
[41] J. A. Mlynek, A. A. Abdumalikov, C. Eichler, and A. Wallraff, Nat. Commun. **5**, 5186 (2014).
[42] The shift from 0 MHz detuning is observed in the absence of the light shift from the tweezer.
[43] The shifts are determined with respect to an offset of $2\pi \times 50$ MHz due to the light shift induced by the tweezer.
[44] J. I. Cirac, P. Zoller, H. J. Kimble, and H. Mabuchi, Phys. Rev. Lett. **78**, 3221 (1997).
[45] L.-M. Duan and H. J. Kimble, Phys. Rev. Lett. **92**, 127902 (2004).
[46] S. Welte, B. Hacker, S. Daiss, S. Ritter, and G. Rempe, Phys. Rev. Lett. **118**, 210503 (2017).
[47] S. Welte, B. Hacker, S. Daiss, S. Ritter, and G. Rempe, Phys. Rev. X **8**, 011018 (2018).
[48] C.-L. Hung, S. M. Meenehan, D. E. Chang, O. Painter, and H. J. Kimble, New J. Phys. **15**, 083026 (2013).
[49] X. Ji, F. A. S. Barbosa, S. P. Roberts, A. Dutt, J. Cardenas, Y. Okawachi, A. Bryant, A. L. Gaeta, and M. Lipson, Optica **4**, 619 (2017).
[50] A. M. Kaufman, B. J. Lester, and C. A. Regal, Phys. Rev. X **2**, 041014 (2012).
[51] J. D. Thompson, T. G. Tiecke, A. S. Zibrov, V. Vuletić, and M. D. Lukin, Phys. Rev. Lett. **110**, 133001 (2013).
[52] Y. Meng, A. Dareau, P. Schneeweiss, and A. Rauschenbeutel, Phys. Rev. X **8**, 031054 (2018).
[53] H. J. Kimble, Nature (London) **453**, 1023 (2008).
[54] E. T. Khabiboulline, J. Borregaard, K. De Greve, and M. D. Lukin, Phys. Rev. A **100**, 022316 (2019).
[55] P. Kómár, E. M. Kessler, M. Bishof, L. Jiang, A. S. Sørensen, J. Ye, and M. D. Lukin, Nat. Phys. **10**, 582 (2014).
[56] J. Borregaard, P. Kómár, E. M. Kessler, M. D. Lukin, and A. S. Sørensen, Phys. Rev. A **92**, 012307 (2015).
[57] N. H. Nickerson, Y. Li, and S. C. Benjamin, Nat. Commun. **4**, 1756 (2013).